Influence of Nanoparticle Addition on the Properties of Wormlike Micellar Solutions

Florian Nettesheim,[†] Matthew W. Liberatore,[‡] Travis K. Hodgdon,[†] Norman J. Wagner,*[,†] Eric W. Kaler,[§] and Martin Vethamuthu[||]

Center for Molecular and Engineering Thermodynamics, Department of Chemical Engineering, University of Delaware, 150 Academy Street, Newark, Delaware 19716, Chemical Engineering Department, Colorado School of Mines, 1613 Illinois Street, Golden, Colorado 80401, Stony Brook University, 407 Administration Building, Stony Brook, New York 11794-1401, and Research and Development Unilever, 40 Merritt Boulevard, Trumbull, Connecticut 06611

Received January 26, 2008. Revised Manuscript Received April 26, 2008

The addition of positively charged, 30 nm diameter silica nanoparticles to cationic wormlike micellar solutions of cetyltrimethylammonium bromide and sodium nitrate is studied using a combination of rheology, small angle neutron scattering, dynamic light scattering, and cryo-transmission electron microscopy. The mixtures are single phase up to particle volume fractions of 1%. The addition of like-charged particles significantly increases the wormlike micelle (WLM) solution's zero shear rate viscosity, longest relaxation time, and storage modulus. The changes are hypothesized to originate from a close association of the particles with the micellar mesh. Small angle neutron scattering measurements with contrast matching demonstrate associations between particles mitigated by the WLMs. The effective interparticle interactions measured by SANS can explain the observed phase behavior. Dynamic light scattering measurements confirm the dynamic coupling of the particles to the micellar mesh.

Introduction

Surfactant molecules self-assemble in solution above the critical micelle concentration (cmc) into micelles. In many cases, these micelles grow into long, semiflexible chains often called wormlike micelles (WLMs).[1−5] The growth of these WLMs depends on surfactant geometry,[6,7] which in the case of ionic surfactants depends on the effective headgroup charge and is, therefore, a function of salt concentration. So-called hydrotropic salts, that is, salts with a hydrophobic moiety, prove very effective to induce rapid micellar growth due to their strong binding to the micelles and therefore the effective screening of the headgroup charge.[4,6] Beyond the overlap concentration, an entangled WLM network is formed and such solutions exhibit viscoelastic properties. Upon the increasing surfactant or salt concentration even further, the entangled network transitions to a branched network and eventually reaches a saturation point leading to phase separation.[4,6,8−14]

The viscoelasticity of these WLM networks at low to intermediate frequencies can often be described by a simple Maxwell model, wherein the stress relaxation is exponential with a single relaxation time λ_r. This response is a direct result of the equilibrium nature of wormlike micelles[2,4,15] which undergo dynamic breakage and recombination on a time scale that is often much faster than the characteristic time of stress relaxation (in the case of polymers, the reptation time). Rheology measurements can therefore be used to study the length and time scales in WLM networks.[16]

Adding nanoparticles or colloids to surfactant solutions, such as lamellar phases,[17−21] can lead to significant changes in macroscopic properties and phase behavior. Colloidal as well as non-Brownian particles are added to WLM solutions at very low concentrations to probe the local structure and viscoelasticity of the network[22−25] in a technique called microrheology.[26,27] In

* To whom correspondence should be addressed. E-mail: wagnernj@udel.edu.
[†] University of Delaware.
[‡] Colorado School of Mines.
[§] Stony Brook University.
[||] Research and Development Unilever.

(1) Nettesheim, F.; Kaler, E. W. Phase Behavior of Systems with Wormlike Micelles. In *Giant Micelles*; Zana, R., Ed.; Taylor and Francis Group: New York, 2007; pp 223−248.
(2) Cates, M. E.; Candau, S. J. *J. Phys.: Condens. Matter* **1990**, *2*(33), 6869–6892.
(3) Cates, M. E. Theoretical Modeling of Viscoelastic Phases. In *Structure and Flow in Surfactant Solutions*; Herb, C. A., Prud'Homme, R. K., Eds.; American Chemical Society: Washington, DC, 1994; Vol. *578*, pp 32−50.
(4) Rehage, H.; Hoffmann, H. *Mol. Phys.* **1991**, *74*(5), 933–973.
(5) Hoffmann, H. Viscoelastic Surfactant Solutions. In *Structure and Flow in Surfactant Solutions*; Herb, C. A., Prud'Homme, R. K., Eds.; American Chemical Society: Washington, DC, 1994; Vol. *578*, pp 231.
(6) Herb, C. A.; Chen, L. B.; Sun, W. M. Correlation of Viscoelastic Properties with Critical Packing Parameter for Mixed Surfactant Solutions in the L1 Region. In *Structure and Flow in Surfactant Solutions*; Herb, C. A., Prud'Homme, R. K., Eds.; American Chemical Society: Washington, DC, 1994; Vol. *578*, pp 153−166..
(7) Isrealachvilli, J. N.; Mitchell, D. J. *Biochim. Biophys. Acta* **1975**, *389*, 13.
(8) Shchipunov, Y. A. *Colloids Surf., A* **2001**, *183*, 541–554.
(9) Raghavan, S. R.; Edlund, H.; Kaler, E. W. *Langmuir* **2002**, *18*, 1056–1064.
(10) Khatory, A.; Kern, F.; Lequeux, F.; Appell, J.; Porte, G.; Morie, N.; Ott, A.; Urbach, W. *Langmuir* **1993**, *9*(4), 933.
(11) Zilman, A.; Kieffer, J.; Molino, F.; Porte, G.; Safran, S. A. *Phys. Rev. Lett.* **2003**, *91*(1), 015901.
(12) Kalur, G. C.; Raghavan, S. R. *J. Phys. Chem. B* **2005**, *109*(18), 8599–8604.
(13) Cristobal, G.; Rouch, J.; Curely, J.; Panizza, P. *Physica A* **1999**, *268*(1−2), 50–64.
(14) Drye, T. J.; Cates, M. E. *J. Chem. Phys.* **1992**, *96*(2), 1367–1375.
(15) Cates, M. E. *J. Phys. Chem.* **1990**, *94*, 371–375.
(16) Schubert, B. A.; Kaler, E. W.; Wagner, N. J. *Langmuir* **2003**, *19*(10), 4079–4089.
(17) Salamat, G.; Kaler, E. W. *Langmuir* **1999**, *15*(16), 5414–5421.
(18) Nettesheim, F.; Grillo, I.; Lindner, P.; Richtering, W. *Langmuir* **2004**, *20*(10), 3947–3953.
(19) Grillo, I.; Levitz, P.; Zemb, T. *Eur. Phys. J. E* **2001**, *5*, 377.
(20) Arrault, J.; Grand, C.; Poon, W. C. K.; Cates, M. E. *Europhys. Lett.* **1997**, *38*(8), 625–630.
(21) Arrault, J.; Poon, W. C. K.; Cates, M. E. *Phys. Rev. E* **1999**, *59*(3), 3242–3252.
(22) Cardinaux, F.; Cipelletti, L.; Scheffold, F.; Schurtenberger, P. *Europhys. Lett.* **2002**, *57*(5), 738.
(23) Bellour, M.; Skouri, M.; Munch, J. P.; Hebraud, P. *Eur. Phys. J. E* **2002**, *8*(4), 431–436.
(24) Hassan, P. A.; Manohar, C. *J. Phys. Chem. B* **1998**, *102*(37), 7120–7125.
(25) Bandyopadhyay, R.; Sood, A. K. *J. Colloid Interface Sci.* **2005**, *283*(2), 585–591.

10.1021/la800271m CCC: $40.75
Published on Web 07/12/2008

these examples, the particles are typically larger than the characteristic length scale of the micelle or micellar network (such as the mesh size) and are used at volume fractions low enough so as not to influence the rheological properties of the micellar network. In one particular study, changes in macroscopic behavior were observed when adding polystyrene particles (particle volume fractions of ~1%) to a like-charged anionic surfactant wormlike micellar system.[28] The authors specifically studied the phase behavior and gel collapse kinetics of the particle micellar mixtures and observed interesting correlations between micellar length and sample stability, leading to the conclusion that the phase behavior of these mixtures is governed by a depletion interaction. In contrast to the study presented here, the polystyrene particles were substantially larger than the mesh size of the wormlike micellar network (R_p = 190 nm, $\xi_m \approx 50$ nm).

In the following, the effects of adding higher concentrations of like-charged nanoparticles to a model WLM solution are investigated. In particular, we explore the question of whether the viscosity of the micellar solutions can be influenced by incorporating particles comparable to or smaller than the mesh size in WLM solutions. Besides being of significant fundamental interest, this question is relevant to applications in personal care and cosmetic products. A stable, single phase regime is identified, and the shear rheological properties, which are both sensitive probes of microstructural changes as well as of practical relevance, are studied as a function of particle volume fraction and network density of the micellar solution. Contrast matching small angle neutron scattering (SANS) experiments are performed to directly identify these microstructural modifications due to the nanoparticle addition as well as to probe the potential of mean force acting between the nanoparticles via the application of liquid state theories. The diffusion of the nanoparticles in the WLM network is studied by dynamic light scattering. Based on these measurements, a hypothesis for nanoparticle addition to the WLM network is proposed. Cryo-transmission electron microscopy provides corroborative evidence for this structuring. A short overview of the most pertinent theoretical results and experimental procedures used is provided prior to presenting and discussing the results.

Theory

Rheology and SANS measurements are combined with models for semiflexible, living polymers to determine the length and time scales of the WLM solutions, as is summarized elsewhere.[16] Only the final relations are presented here: The Cates model[14,15,29] for the dynamics of WLMs considers two primary relaxation times associated with the reptation of a micelle, λ_{rep}, and micellar breakage, λ_{br}. In the limit of fast breakage ($\lambda_{br} \ll \lambda_{rep}$), this leads to Maxwellian linear viscoelastic rheology with a single relaxation time as the geometric mean of λ_{rep} and λ_{br}:

$$\lambda_r = \sqrt{\lambda_{rep}\lambda_{br}} \tag{1}$$

This mean relaxation time is identified with the crossover in the viscoelastic spectra. The frequency where $\omega = \lambda_{br}^{-1}$ corresponds to a local minimum in G'', which also defines the plateau modulus G_p'. Rubber elasticity relates the mesh size ξ_M directly to the plateau modulus and the network density ν as

$$G_p' = \nu k_B T \propto \frac{k_B T}{\xi_M^3} \tag{2}$$

The loss modulus at the minimum is related to the contour length $\bar{L}$ and entanglement length l_e as

$$\frac{G_p'}{G_{min}''} \approx \frac{\bar{L}}{l_e} \tag{3}$$

The entanglement length is related to the mesh size and persistence length by

$$l_e \approx \frac{\xi_M^{5/3}}{l_p^{2/3}} \tag{4}$$

The persistence length l_p can be measured by using, for example, flow birefringence,[30] static and dynamic light scattering,[31–33] high frequency rheology,[34,35] or neutron spin echo measurements.[36]

The scattering of WLMs can be described by the form factor of a semiflexible chain (SFC) taking excluded volume effects into account.[37,38] At high scattering vectors, q, the spectra exhibit oscillations resulting from the cross-sectional dimension of the WLM. At intermediate q, the intensity decreases as q^{-1}, which is a signature of linearly extended rigid objects such as wormlike micelles. At lower q, there is a transition to a regime where the intensity changes as $q^{-1.5}$ to q^{-2}. The scattering vector at which this transition occurs is approximately the inverse of the persistence length l_p. Network density fluctuations and interparticle correlations often lead to strong deviations from simple SFC scattering at lower scattering vectors in the form of correlation peaks.

For mixed systems of wormlike micelles and particles, the scattering is a convolution of scattering from both components in terms of partial structure factors.[39,40] With contrast matching by selective deuteration, these partial structure factors are determined.[41] Here, we consider two limits achieved by varying the H_2O/D_2O ratio in the suspending medium, namely particle matching such that only the WLMs are evident and WLM matching such that the spatial arrangement of the particles is probed.

A model for the interparticle interactions employed herein is the idealized square well potential (SQW), for which phase diagrams are readily available.[42–44] For a SQW fluid of particles with a hard sphere radius of R_{hs}, the potential is defined as

(26) Mason, T. G.; Ganesan, K.; van Zanten, J. H.; Wirtz, D.; Kuo, S. C. *Phys. Rev. Lett.* **1997**, *79*(17), 3282–3285.
(27) MacKintosh, F. C.; Schmidt, C. F. *Curr. Opin. Colloid Interface Sci.* **1999**, *4*(4), 300–307.
(28) Petekidis, G.; Galloway, L. A.; Egelhaaf, S. U.; Cates, M. E.; Poon, W. C. K. *Langmuir* **2002**, *18*(11), 4248–4257.
(29) Spenley, N. A.; Cates, M. E.; McLeish, T. C. B. *Phys. Rev. Lett.* **1993**, *71*(6), 939–942.
(30) Shikata, T.; Dahman, S. J.; Pearson, D. S. *Langmuir* **1994**, *10*, 3470–3476.
(31) Farge, E.; Maggs, C. *Macromolecules* **1993**, *26*, 5041.
(32) Zilman, A.; Granek, R. *Phys. Rev. Lett.* **1996**, *77*(23), 4788.
(33) von Berlepsch, H.; Harnau, L.; Reineker, P. *J. Phys. Chem. B* **1998**, *102*, 7518–7522.
(34) Willenbacher, N.; Oelschlaeger, C.; Schoepfer, M.; Fischer, P.; Cardinaux, F.; Scheffold, F. *Phys. Rev. Lett.* **2007**, *99*, 068302.
(35) Willenbacher, N.; Oelschlaeger, C. *Curr. Opin. Colloid Interface Sci.* **2007**, *12*(1), 43–49.
(36) Nettesheim, F.; Wagner, N. J. *Langmuir* **2007**, *23*, 5267.
(37) Pedersen, J. S.; Schurtenberger, P. *Macromolecules* **1996**, *29*, 7602.
(38) Pedersen, J. S.; Laso, M.; Schurtenberger, P. *Phys. Rev. E* **1996**, *54*(6), R5917–R5920.
(39) Klein, R. Interacting Colloidal Suspensions. In *Neutrons, X-rays and Light: Scattering Methods Applied to Soft Condensed Matter*, 1st ed.; Lindner, P., Zemb, T., Eds.; Elsevier: Amsterdam, 2002; pp 351−380.
(40) Kline, S. R.; Kaler, E. W. *J. Chem. Phys.* **1996**, *105*(9), 3813–3822.
(41) Schurtenberger, P. Contrast and Contrast Variation in Neutron, X-ray and Light Scattering. In *Neutrons, X-rays and Light: Scattering Methods Applied to Soft Condensed Matter*, 1st ed.; Lindner, P., Zemb, T., Eds.; Elsevier: Amsterdam, 2002; pp 145−170.

$$U(r) = \begin{cases} \infty & r \leq 2R_{hs} \\ -\varepsilon & 2R_{hs} \leq r \leq 2R_{hs}\lambda \\ 0 & r \geq 2R_{hs}\lambda \end{cases} \quad (5)$$

Here, ε is the depth of the potential in units of k_BT and λ is the relative width with

$$\lambda = 1 + \frac{\Delta}{R_{hs}} \quad (6)$$

The resulting structure factor was derived by Sharma and Sharma,[45] and it is implemented within the SANS analysis package available through NIST.[46]

Dynamic light scattering (DLS) is performed to probe the diffusive motion of the nanoparticles in the WLM solutions. As both components scatter light, two modes are observed in the field-correlation function measured by DLS.[47] As a first approximation, these modes can be described by a simple model of diffusion of a sphere through a viscous continuum. The composite field-correlation function $g_t(\tau)$ is simply

$$g_t(\tau) = A\, g_m(\tau) + (1 - A)\, g_p(\tau) \quad (7)$$

where $g_m(\tau)$ is the field-correlation function of the WLM solution in the absence of the particles, which is obtained from the measured intensity autocorrelation function by using the Siegert relation. $g_p(\tau)$ is the field-correlation function for a diffusing sphere calculated using the Stokes−Einstein relation $D_0 = k_BT/6\pi\eta_sR_h$, and $g_p(\tau) = \exp(-Dq^2\tau)$. As the hydrodynamic radius of the particle is measured independently, the only adjustable parameter is the apparent viscosity of the medium. Thus, this approach can be used to probe the local effective viscosity of the suspending medium around the particle.

Experimental Section

Samples were prepared from cetyltrimethylammonium bromide (CTAB) sodium nitrate ($NaNO_3$) in distilled, deionized water to which the silica particles were added in the form of the supplied stock solution. Surfactant and salt were purchased from Aldrich and used as received. $NaNO_3$ is not a hydrotrope, so its addition to CTAB only leads to moderate micellar growth. $NaNO_3$ was selected because hydrotropes such as NaSal strongly interact with the silica particles and cause their flocculation. In the series of monovalent counterions examined, NO_3^- produced samples with the lowest Krafft temperature of 22 °C. The silica particles with a positive surface charge and a diameter of 30 nm were provided by AZ Electronics Co. in the form of 30 wt % dispersions with a density of 1.2 g/cm^3 and the silica particles having a dry density of 2.2 g/cm^3. Samples were vortex mixed and left to equilibrate overnight. All experiments were performed at 25 °C unless otherwise noted.

As a control experiment, supernatant from the stock particle solution was obtained by centrifugation, and comparable WLM mixtures were prepared without the silica phase to examine the effects of the electrolyte present in the colloidal dispersion on the WLM solution's structure and rheology. The rheological properties of this control were found to be indistinguishable from those of the pure WLM solution at the same surfactant concentration. Therefore, changes in properties of the WLM mixtures with particles are due to the presence of the particles and are not a result of added electrolyte.

The stability of the particle dispersions was observed by visually inspecting sealed, quiescent samples over several months. All samples of particle volume fractions up to 1% were stable over the period of inspection. Particle volume fractions above 1% were observed to develop an opaque sediment and a clear, low viscosity supernatant, indicating a loss of stability on the time scale of days.

Rheological data were collected using a stress-controlled AR-G2 rheometer (TA instruments) in cone-and-plate geometry (4°, 40 mm). Dynamic light scattering (DLS) was performed on a Brookhaven instrument equipped with a goniometer allowing angle dependent measurements at a wavelength of 488 nm.

Neutron scattering experiments were performed at the NG-3 and NG-7 beamlines at the NIST Center for Neutron Research (NCNR) at the National Institute for Standards and Technology (NIST). To obtain sufficient scattering contrast, H_2O was replaced by D_2O (Cambridge Isotopes). For the contrast variation measurements, two different H_2O/D_2O mixtures were prepared as suspending media. A 35:65 (w/w) H_2O/D_2O mixture was used to match the scattering of the silica spheres, and a 95:5 (w/w) H_2O/D_2O mixture was used to match the scattering of the micelles. In the case of matching the silica spheres, the suspending medium composition was calculated from the density of silica (2.2 g/cm^3) and the scattering length densities of the components at a wavelength of 6 Å. In the case of matching the surfactant $I(0)$, was measured for a series of WLM solutions in suspending mediums with 70−100 wt % H_2O to determine the match point. Data were corrected for background scattering, normalized using standard procedures, and averaged using software provided by NIST.[46,48,49]

Samples for cryo transmission electron microscopy (cryo-TEM) were examined using a Techni 12 transmission electron microscope at an acceleration voltage of 120 keV. Specimens were prepared using a Vitrobot Mark II instrument. Quantifoil grids were submerged in the liquid sample, blotted to produce a thin liquid film, and allowed adequate relaxation time before vitrification in liquid ethane held at its freezing temperature. Grids were held below −170 °C during investigation in the transmission electron microscope, and images were recorded using a Gatan multiscan charge-coupled device (CCD) camera and processed with Digital Micrograph software.

Results

Sample Stability. Samples were prepared over a range of surfactant and salt concentrations, and various amounts of particles were included. The phase diagrams were determined by visual inspection in water baths at $T = 25 \pm 1$ °C. Figure 1 presents the results at three ratios of salt to surfactant concentrations (c_s/c_d) where the nanoparticle volume fraction and salt concentrations are varied. Increasing particle volume fraction (Φ_p) or surfactant concentrations (c_d) leads to phase separation into an opaque soft sediment and a low viscosity supernatant. As the ratio of salt to surfactant increases, the unstable region expands. The samples separate into a particle rich sediment and particle free supernatant. This transition is thermally reversible. This was tested for a solution of 40 mM CTAB and 140 mM $NaNO_3$, and the transition temperature was found to be about 40 °C. Structural and rheological measurements were only made on samples that did not phase separate during the time of experimentation, that is, on time scales of several days. Note that the sample at 1 vol % particles eventually phase separated, but this process was on the order of several months.

Rheology. The influence of nanoparticle addition on the rheological properties of wormlike micellar solutions was studied using a 100 mM CTAB/200 mM $NaNO_3$ sample containing 0.1, 0.5, and 1 vol % silica particles (Figures 2 and 3). The neat WLM solution (no silica particles) exhibits a plateau at low shear rates

(42) de Kruif, C. G.; Rouw, P. W.; Briels, W. J.; Duits, M. H.; Vrij, A.; May, R. P. *Langmuir* **1989**, *5*, 422.
(43) Kiselev, S. B.; Ely, J. F.; Elliott, J. R. *Mol. Phys.* **2006**, *104*(15), 2545–2559.
(44) Bergenholtz, J.; Wu, P.; Wagner, N. J.; Daguanno, B. *Mol. Phys.* **1996**, *87*(2), 331–346.
(45) Sharma, R. V.; Sharma, K. C. *Physica A* **1977**, *89*(1), 213–218.
(46) Kline, S. R. *J. Appl. Crystallogr.* **2006**, *39*(6), 895.
(47) Nemoto, N.; Kuwahara, M.; Yao, M. L.; Osaki, K. *Langmuir* **1995**, *11*(1), 30–36.
(48) Glinka, C. J.; Barker, J. G.; Hammouda, B.; Krueger, S.; Moyer, J. J.; Orts, W. J. *J. Appl. Crystallogr.* **1998**, *31*, 430–445.
(49) Barker, J. G.; Pedersen, J. S. *J. Appl. Crystallogr.* **1995**, *28*, 105–114.

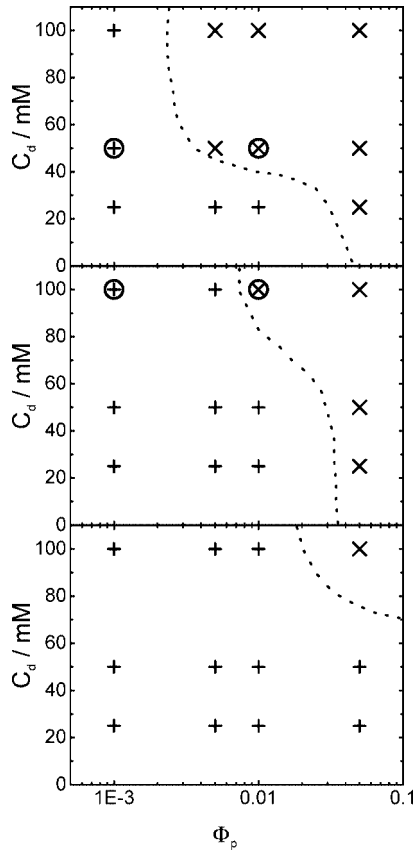

Figure 1. Stability diagram of the particle dispersions in various wormlike micellar solutions of CTAB and $NaNO_3$ as a function of both surfactant and electrolyte concentration (bottom, $c_s/c_d = 1$; middle: $c_s/c_d = 2$; top, $c_s/c_d = 3$). The (+) symbols represent samples that appear as single phase, and the (×) symbols represent samples that have separated after an equilibration time of about 12 months. The circled symbols indicate samples investigated in more detail in this study. It has to be noted that even the higher particle volume fraction is stable for several days, sufficient to perform experiments.

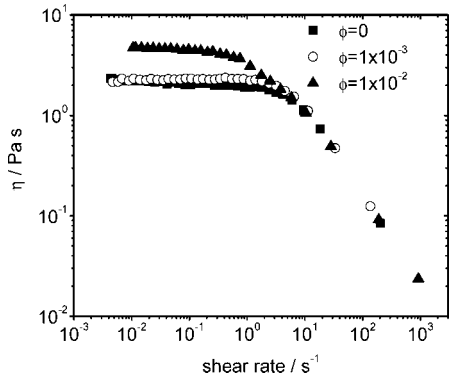

Figure 2. Steady state viscosity of a wormlike micellar solution of 100 mM CTAB and 200 mM $NaNO_3$ as a function of silica volume fraction.

and significant shear thinning at shear rates above 5 s^{-1}. The onset of shear thinning at a shear rate $\dot{\gamma}^*$ identifies the relaxation time λ_r ($\dot{\gamma}^* = \lambda_r^{-1}$). The relaxation times and zero shear viscosities were obtained by fitting a Carreau model[50] to the shear viscosity.

The surfactant solution exhibits moderate viscoelasticity, as seen in Figure 3. The lines represent fits to a Maxwell fluid

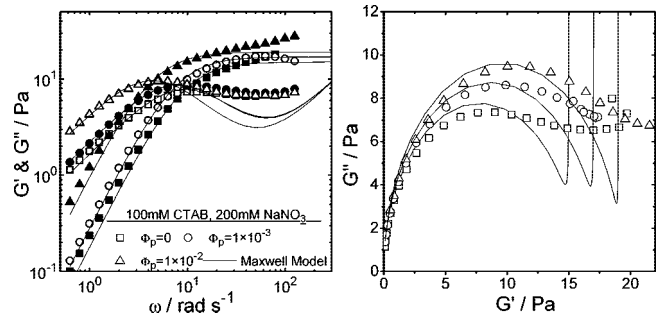

Figure 3. Linear viscoelastic spectrum of 100 mM CTAB and 200 mM $NaNO_3$ as a function of silica volume fraction and Cole−Cole representations of the same data. Lines represent fits to the Maxwell model.

Table 1. Rheological Parameters of 100 mM CTAB and 200 mM $NaNO_3$ in H_2O

100 mM CTAB/ 200 mM $NaNO_3$	no particles	$\Phi_p = 0.001$	$\Phi_p = 0.01$
η_0/Pa·s	2.1	2.3	4.5
($G_0\lambda_r$/Pa·s)	(2)	(2.3)	(5.1)
λ_r/s	0.19	0.17	1.05
G_0'/Pa	17	17.4	23.2
G_{min}''/Pa	6.6	7	6.5
l_p/nm	24	24	24
ξ_m/nm	62	62	56
l_e	120	120	100
L_c	310	310	350
λ_r/s (dyn. exp.)	0.12	0.13	0.22
λ_{br}/s (dyn. exp.)	0.016	0.016	0.016
λ_{rep}/s (dyn. exp.)	0.9	1.1	3.0

model with an additional term to account for the high frequency deviations from the simple form of the Maxwell model. Such deviations at frequencies above the crossover frequency indicate that the semiflexible surfactant micelles are relatively short. Thus, the longest bending modes of the micelles are significant at frequencies just above the longest relaxation time. The Cole−Cole plot (Figure 3) demonstrates the expected deviations from Maxwellian behavior at higher frequencies and identifies the breakage time as the local minimum in G''. Table 1 summarizes the length and time scales extracted from these data, where the persistence length is taken to be 24 nm.[30,51]

Adding just $\Phi_p = 0.001$ of nanoparticles does not substantially change the shear viscosity or plateau modulus, and only a slight shift of the crossover frequency to a lower value is observed. The measurement of λ_{br} from the minimum in G'' is difficult, especially for the pure WLM sample. However, no significant change in the position of the minimum is observed upon further particle addition, and it is therefore assumed to remain largely unchanged. Thus, the observed increase in λ_r upon nanoparticle addition is primarily due to an increase in λ_{rep}.

Significant changes occur upon adding $\Phi_p = 0.01$ of nanoparticles. The zero shear rate viscosity increases by a factor of nearly 2, and the onset of shear thinning shifts to lower shear rates. The dynamic measurements show an increase in both plateau modulus and reptation time. However, the breakage times do not change, within measurement accuracy, with nanoparticle addition. A comparative summary of all the length and time scales is given in Table 1.

(50) Macosko, C. W. *Rheology, Principles, Measurements, and Applications*; Wiley-VCH: New York, 1994.

(51) Shikata, T.; Pearson, D. S. Rheo-optical Behavior of Wormlike Micellar Systems. In *Structure and Flow in Surfactant Solutions*; Herb, C. A., Prud'Homme, R. K., Eds.; American Chemical Society: Washington, DC, 1994; Vol. *578*, pp 129−139.

Table 2. Rheological Parameters of 50 mM CTAB and 150 mM $NaNO_3$ in H_2O

50 mM CTAB/ 150 mM $NaNO_3$	no particles	$\Phi_p = 0.001$	$\Phi_p = 0.005$	$\Phi_p = 0.01$
η_0/Pa·s	0.03	0.05	0.21	0.75
($G_0\lambda_r$/Pa·s)				0.625
λ_r/s	0.01	0.05	0.37	0.75
G_0'/Pa				2.5
G_{min}''/Pa				1.4
l_p/nm				24
ξ_m/nm				120
l_c/nm				340
L_c/nm				610
λ_r/s (dyn. exp.)				0.25
λ_{br}/s (dyn. exp.)				0.05
λ_{rep}/s (dyn. exp.)				1.25

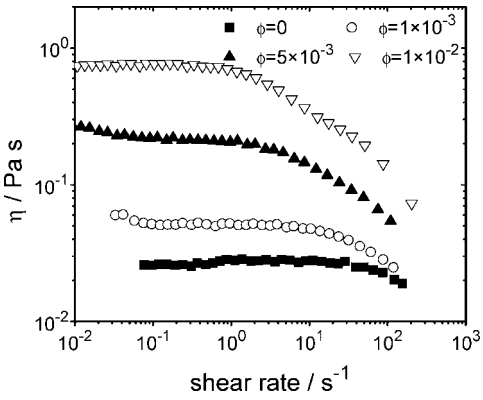

Figure 4. Steady state viscosity of a wormlike micellar solution of 50 mM CTAB and 150 mM $NaNO_3$ as a function of silica volume fraction.

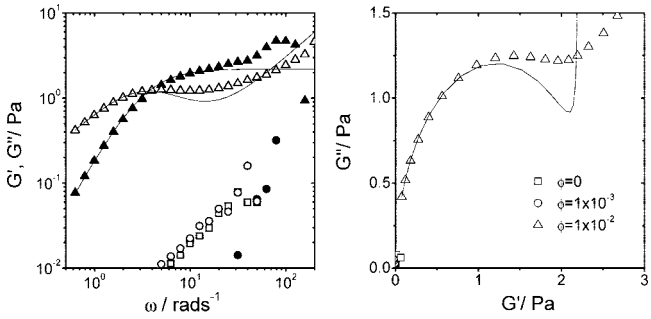

Figure 5. Linear viscoelastic spectrum of 50 mM CTAB and 150 mM $NaNO_3$ as a function of silica volume fraction and Cole−Cole representations of the same data. Lines represent fits to the Maxwell model.

As only 1 vol % particle addition greatly increases the solution's viscoelastic properties, a more dilute WLM solution, 50 mM CTAB/150 mM $NaNO_3$, with a lower network density was similarly examined (Table 2). At this low surfactant concentration, the WLM solution does not exhibit any viscoelasticity and its viscosity is only about 30 times that of water. The sample does display weak shear thinning (see Figures 4 and 5). Here, even adding $\Phi_p = 0.001$ has a noticeable effect on the shear viscosity, and with the addition of $\Phi_p = 0.01$ the sample is noticeably viscoelastic. Note that, with only 1 vol % nanoparticles added, the zero shear rate viscosity increases by a factor of 25.

Small Angle Neutron Scattering. SANS measurements were performed on the 100 mM CTAB/200 mM $NaNO_3$ sample with and without nanoparticles under three contrast conditions, namely full (pure D_2O), micelle and nanoparticle contrast as defined above.

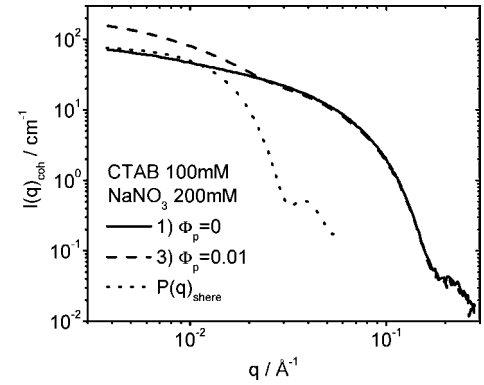

Figure 6. Coherent scattering intensity of 100 mM CTAB/200 mM $NaNO_3$ in D_2O with (dashed line) and without (solid line) 1 vol % silica particles. The dotted line represents the form factor of a sphere of mean radius 15 nm with a Schulz size distribution with a standard deviation of 10%.

The pure WLM sample in full contrast displays the typical features of a semiflexible chain (Figure 6). The scattering at high q can be fit by a cylindrical form factor yielding the cross-sectional radius r_{cs} of 2.5 nm. In agreement with the cylindrical symmetry of the WLM, the slope in the intermediate q-range is close to −1. This region is, however, not very pronounced, which could be the result of network correlations that lead to a decrease in intensity at lower q as well as the relatively short contour length. The correlation length of the 100 mM CTAB/200 mM $NaNO_3$ sample is known from the plateau modulus from dynamic rheology to be on the order of 60 nm. Thus, correlations at $q > 2\pi/\xi_m = 0.01$ Å^{-1} are expected to lead to a reduction in scattering intensity.

At high scattering vectors ($q \geq 3 \times 10^{-2}$ Å^{-1}), the addition of nanoparticles does not affect the scattered intensity, and thus, the micellar structure on length scales of r_{cs} up to ∼20 nm remains unperturbed. At lower scattering vectors, an increase in scattered intensity with nanoparticle addition is observed, as expected. The form factor for a sphere of 15 nm mean radius with a Schulz size distribution with a standard deviation of 10% is also shown for reference in Figure 6. Clearly, the increase in scattering intensity for the mixture at lower scattering vectors is consistent with the presence of dispersed nanoparticles contributing to the overall scattering intensity.

To determine whether the presence of particles has any influence on the micelle network structure, contrast matching of the nanoparticles was performed using a 39 wt % mixture of H_2O in D_2O with 1 vol % silica particles. Under these conditions, only the micelles in the mixture scatter. Figure 7 compares this measurement to that from the pure wormlike micelles in D_2O. The preservation of local structure is confirmed at high q ($q \geq 6 \times 10^{-2}$ Å^{-1}). The only effect of the nanoparticles on the micelle structure apparent in the SANS measurements is a weak suppression in the low q scattering intensity.

Contrast matching the micelles using 95 wt % H_2O in D_2O as the suspending medium probes the spatial arrangement of the nanoparticles in the WLM solution. Figure 8 compares the scattering of 0.1 and 1 vol % silica particles in 100 mM CTAB/200 mM $NaNO_3$ using 95 wt % H_2O in D_2O as the suspending medium along with the scattering of the silica particles at 1 vol % in D_2O. In the presence of the WLMs, the nanoparticle scattering shows evidence of an upturn at low scattering vectors indicative of weak attractive interactions.

The intensity was fit to a polydisperse but homogeneous sphere model using a form factor comprising a Schultz size

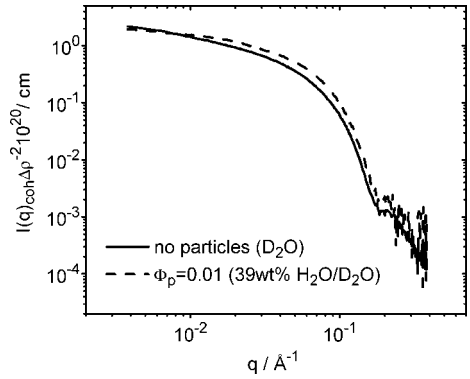

Figure 7. Scattering cross section of 100 mM CTAB/200 mM $NaNO_3$ in D_2O compared to 100 mM CTAB/200 mM $NaNO_3$ with 1 vol % silica particles in 39 wt % H_2O/D_2O.

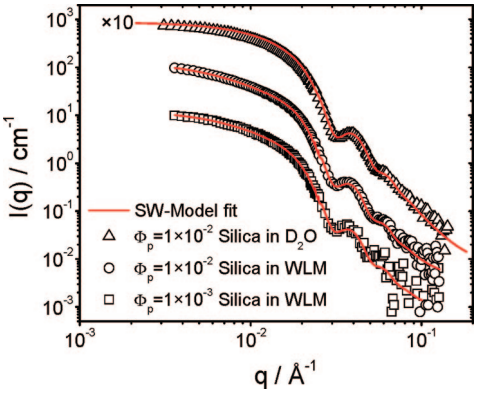

Figure 8. Coherent scattering cross sections of $\Phi_p = 0.001$, $\Phi_p = 0.01$ silica in 100 mM CTAB/200 mM $NaNO_3$/39 wt % H_2O/D_2O, and pure silica in D_2O ($\Phi_p = 0.01$). The lines represent a fit of the scattering to a square well structure according to the structure factor of Sharma and Sharma[34] using a Schultz distribution for the particle radius. For details of this analysis, see the text and Table 3.

distribution with a standard deviation in size of 10%. The incoherent background was included as a floating parameter. The structure factor calculated from liquid state theory using a square well potential was used to describe particle−particle interactions.[45] The fits are shown in Figure 8, and the parameters are listed in Table 3. Note that the particle radius (r) determined from the fit increases by 0.5 nm in the presence of surfactant, presumably due to surfactant adsorption. Interestingly, a weak square well attraction was required to accurately describe the nanoparticle scattering in D_2O, suggesting some weak attractions are evident due to ubiquitous London−van der Waals interactions. To simplify the fitting and enable comparison between the data sets, a square well width of $\lambda = 1.375$ was found to best describe all three measurements and so only the strength of the attraction (well depth) was varied between the samples. The scattering length density of the particles was calculated using the measured density of 2.2 g/cm^3 for silica, and the suspending medium's scattering length density was calculated from the reported densities and the composition. A 10% adjustment in scattering length density was allowed for the mixtures in WLM solutions, partly to account for the added suspending medium from the nanoparticle stock solution. Thus, the only fit parameter in the modeling shown in Figure 8 is the depth of the square well potential (ε/k_BT), eq 5; the parameters are summarized in Table 3.

Discussion

Nanoparticle addition to wormlike micellar solutions, where the particles are of the same charge as the surfactant, leads to stable solutions at low particle concentrations. At high particle volume fractions, reversible phase separation is observed with the formation of a dense, soft solid precipitate. In the stable, one phase regime, nanoparticle addition increases both the zero shear rate viscosity and the storage modulus. Indeed, we have demonstrated that nanoparticle addition can even create viscoelasticity in dilute, unentangled WLM solutions. For viscoelastic WLM solutions, particle addition moves the crossover frequency to lower frequencies, but the position of the minimum in G'' remains roughly constant. Particle contrast matching SANS measurements show that adding nanoparticles slightly decreases the forward scattering from the micelles whereas the structure of the micellar solutions on the length scale of the worm cross section remains unchanged. Surfactant contrast matching SANS measurements indicate that the particles are dispersed but have an apparent attractive particle−particle interaction mediated by the WLMs. The diffusion of the particles in the mesh as measured by DLS (see the Supporting Information) is significantly hindered as compared to that expected from a medium with the zero shear rate viscosity of the bulk WLM solution.

To explain these observations, we hypothesize that the nanoparticles physically participate in the WLM network as shown in Figure 9. Despite being like-charged as the surfactant, hydrophobic interactions between the cationic surfactant and the net positively charged nanoparticle can drive adsorption. In particular, WLMs grow linearly with the addition of surfactant because of the unfavorable energy of formation of endcaps relative to cylinders. Consequently, it is plausible that the nanoparticles would first associate with the energetically unfavorable endcaps, and therefore, it is plausible that the nanoparticles become "junctions" between WLMs.

This simple physical picture of nanoparticle−micelle association is consistent with the static and dynamic data presented herein and the cryo-TEM micrographs in the Supporting Information. Reversible phase separation at higher nanoparticle concentrations can be simply a consequence of the particle−particle attractions mediated by the WLMs. These attractions are envisioned to be similar to those observed in polymer bridging.[52] Indeed, phase separation is promoted by the addition of salt, which leads to micellar growth and hence stronger bridging attractions (note that the nanoparticles are stable at these salt concentrations in the absence of surfactant). Three additional physical observations were made that are relevant to this discussion. First, anionic silica particles of similar composition were inherently unstable in the cationic WLM solutions, as expected. Second, larger silica nanoparticles with a diameter of 50 nm and similar surface potential were also not stable in the cationic WLMs. Third, the addition of hydrotropic salts, which generate longer worms by increasing the energy difference for endcap formation relative to the formation of cylinders, also resulted in phase separation over the range of particle, surfactant, and salt concentrations examined here. Thus, these observations of phase separation are suggestive of effective attractions between the particles introduced by the presence of the micelles.

Depletion interactions arising from the WLMs could potentially be a source of attractive interactions leading to possible phase separation without surfactant adsorption onto the nanoparticles.[28] However, depletion interactions at the low particle loadings are too weak in comparison to the viscoelasticity of the WLM solution

(52) Bhatia, S. R.; Russel, W. B. *Macromolecules* **2000**, *33*, 5713.

Table 3. Square Well Fit Parameters to the Scattering Profiles of Silica Particles

	silica in D_2O, $\Phi_p = 0.01$	silica in 100 mM CTAB/200 mM $NaNO_3$, $\Phi_p = 0.001$	silica in 100 mM CTAB/200 mM, $NaNO_3$, $\Phi_p = 0.01$
η_{SW}	0.01	0.001	0.01
$\langle R_{hs} \rangle$ (nm)[54]	14.4	14.9	14.9
$\sigma/\langle R_{hs} \rangle$	0.1	0.1	0.1
SLD_p (Å^{-2})	3.6×10^{-6}	3.6×10^{-6}	3.6×10^{-6}
SLD_s (Å^{-2})	6×10^{-6}	1.34×10^{-6}	1.45×10^{-6}
ε/k_BT	1.19	29.32	4.14
$\lambda = (1 + \Delta/\langle R_{hs} \rangle)$	1.375	1.375	1.375
background (cm^{-1})	0.095	0.4	0.4

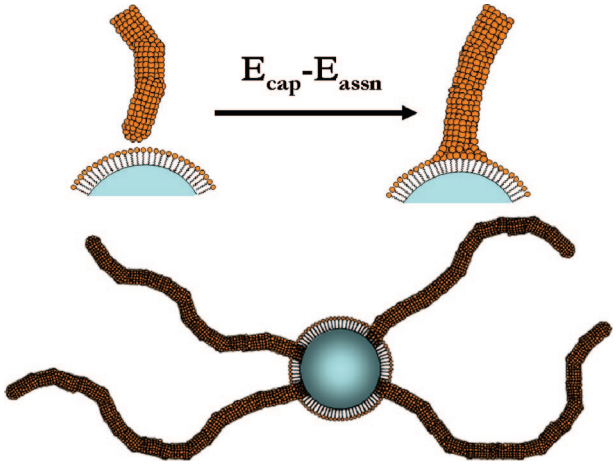

Figure 9. Sketch of micelle particle association based on the replacement of an endcap by a silica nanoparticle (top) and the resulting network junction (bottom).

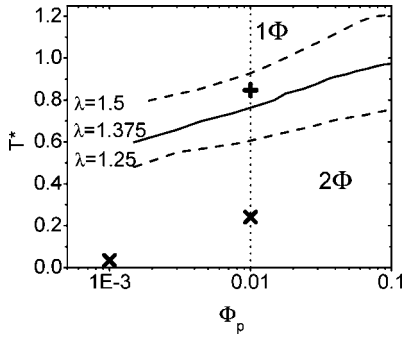

Figure 10. Theoretical phase diagram of a square well fluid with $\lambda = 1.375$ taken from Kiselev et al.[36] The lines for $l = 1.25$ and 1.5 are shown for reference. The results of a square well fit to the data of bare silica particles in D_2O (+) and silica particles dispersed in the wormlike micellar mesh (×) are depicted in the phase diagram.

to result in the significant increases in viscoelasticity. Nanoparticles materially participating in the WLM network, on the other hand, can enhance the WLM network viscoelasticity and would lead to a substantial retardation of the nanoparticle mobility. WLM anchoring onto the nanoparticles also leads to a dependence of the sample stability on the connectivity of the particles, that is, the available surface area for micellar adsorption per particle,[53] whereby larger particles should phase separate more easily, as observed. As significantly, manipulating the added salt concentrations leads to micellar growth and later phase separation in the presence of WLMs.

The rheological behavior provides quantitative insight, as changes in viscosity and elasticity can be connected to microstructural changes. The increase in zero shear rate viscosity upon the addition of 1 vol % silica particles cannot be accounted for by particles that freely diffuse through the network. The Einstein relation predicts that addition of 1 vol % of a colloid would increase the viscosity by 2.5% instead of the 300% increase observed. The enhancement of the plateau storage modulus upon nanoparticle addition can be interpreted as an increase in network density, that is, by assuming that the silica nanoparticles act as new network junctions. A simple estimate illustrates that the observed increase is in semiquantitative agreement with this physical picture. From eq 2, the network density ν of the pure 100 mM CTAB/200 mM $NaNO_3$ micellar system is 4×10^{21} m^{-3}. A nanoparticle volume fraction of $\Phi_p = 0.01$ corresponds to a number density of 0.7×10^{21} m^{-3}. Thus, if each particle served as a new network junction, this would account for a 20% increase in G_p', which compares well with the observed 30% increase (Table 1). Alternatively, one can estimate the mesh volume from rheology, and the change in the plateau modulus should then correspond to a change in particles per mesh volume. This number turns out to be 0.1 for this sample, indicating that only a fraction of junctions is established by the particles.

Considering the more dilute WLM system of 50 mM CTAB that is below the entanglement conditions in the absence of nanoparticles, the strong viscoelasticity arising upon addition of only 1% nanoparticles is consistent with the nanoparticles bridging WLMs and participating in the WLM network. Here again, the measured plateau modulus of the order of 2 Pa is quantitatively consistent with the number of nanoparticles present. Assuming that each particle forms a network junction, one would expect $G_p' = 3$ Pa. Since the pure WLM solution does not exhibit any elasticity, hence one should expect the particle per mesh volume to be very close to unity. However, the value is 1.4, indicating that some particles do not contribute to network formation. On the other hand, it is not possible to explain these strong increases in viscoelasticity by considering only stress contributions from dispersed nanoparticles at these concentrations (the viscosity of a 1% particle dispersion has a viscosity of 1.14 mPa·s, very close to the Einstein prediction); that is, they must modify the WLM network directly to have this significant impact on the stress.

The terminal relaxation time determined from the crossover of G' and G'' increases with nanoparticle addition in accordance with the increase in zero shear rate viscosity and the plateau value of G'. As the breakage time of the micelles does not change significantly, the increase in the terminal relaxation time is a consequence of an increase in reptation time. The reptation time strongly increases with the molecular weight of a wormlike micelle (of the order of L_c^3), and so the creation of longer micelles through nanoparticle bridging of micellar endcaps will significantly increase the terminal relaxation time of the solution. The reptation time increasing by about a factor of 3 (Table 1) would require only a modest increase in the effective contour length L_c by nanoparticle bridging. It is plausible that nanoparticles bridging the wormlike micelles would not significantly influence the breakage time, because $\lambda_{br} \propto L_c^{-1}$, which is a much weaker

dependence and probably not resolvable given the uncertainty in the measurement.

SANS measurements on the mixtures demonstrate that the nanoparticles are dispersed in the WLM network and that the WLMs themselves remain unchanged on the length scale problems. Contrast matching the nanoparticles demonstrates that nanoparticle addition leads to a decrease in low q intensity. Although there is no theory to directly connect this change in WLM scattering to the viscosity, results of mode-coupling theory for suspensions can provide some guidance,[53] where the solution's viscosity is shown to scale in proportion with the square root of the solution's osmotic compressibility $\eta \propto (\partial\Pi/\partial c)^{1/2}$. This in turn is inversely related to the measured scattering at zero wave vector: $I(0) \propto (\partial\Pi/\partial c)^{-1}$, such that the scattering intensity at zero wave vector, when properly corrected for changes in scattering length density associated with isotope substitution, can be approximated as $\eta \propto 1/(I(0))^{1/2}$. From the results shown in Figure 7 and correcting for the scattering length difference due to changes in the suspending medium, the results suggest that the reduction in forward scattering upon addition of 1 vol % nanoparticles should lead to an increase in the zero shear rate viscosity of the micellar phase by ~3 times that in the absence of nanoparticles. The measured ratio (Table 1) is 2.1, in reasonable agreement, which suggests the observed increase in viscosity upon nanoparticle addition is due to modifications of the micellar network structure.

The parameters obtained from fitting the SQW structure factor to the surfactant contrast matched SANS data can be used to estimate the phase behavior of the of nanoparticle WLM mixtures. The first order gas−liquid coexistence curve for square well fluids with well widths of $\lambda = 1.375$ has been calculated,[43] and it is reproduced in Figure 10, where the measured well depth is used to calculate the dimensionless temperature $T^* = \varepsilon/k_BT$. The coexistence lines for $\lambda = 1.25$ and 1.5 well widths are provided for reference to demonstrate the sensitivity of the phase behavior to the potential parameters. The square well model predicts phase separation for these fluids, which is observed after several months. Note that the samples are kinetically stable for weeks and the SANS and rheology experiments were performed within a few days of sample preparation when the sample was in a single phase. Given the crude approximation of the potential by a square well and the sensitivity of the coexistence curve to the shape of the potential, we can only conclude from these three SANS measurements that the physical picture of a potential of mean force acting between the nanoparticles due to WLM bridging is physically reasonable. A more quantitative connection requires developing a potential appropriate for WLMs that, unlike the existing models for polymer bridging, can break and reform and a complementary calculation of the phase equilibria for this potential model.

Finally, the DLS measurements (Supporting Information) demonstrate that the mixture has dynamics consistent with the fast modes of the WLMs, which remain unchanged upon nanoparticle addition, as well as the slow modes that indicate greatly hindered nanoparticle diffusion. The fast wormlike chain dynamics are not affected by the presence of the nanoparticles, consistent with the SANS studies showing no structural changes on length scales of ~20 nm or less. However, a simple analysis of the autocorrelation functions (ACFs) provides an estimate of the local viscosity probed by the nanoparticles, which is substantially larger than the zero shear rate viscosity of the WLM network itself and over double that of the zero shear rate viscosity of the mixture. This significant increase in local viscosity probed by the nanoparticles shows that they are not simply freely diffusing through the mesh defined by the WLMs, but rather, that they must materially be incorporated into the WLM network, as also suggested by the cryo-TEM micrographs (Supporting Information).

Conclusions

The addition of nanoparticles of like charge to a cationic wormlike micellar solution leads to significant increases in viscosity and viscoelasticity and, at particle loadings of only a few percent, to thermodynamic phase separation. Indeed, nanoparticles can structure low viscosity, weakly entangled WLM solutions to become viscoelastic. The increases in viscoelasticity can be quantitatively accounted for by assuming that the nanoparticles incorporate into the WLM network and thereby increase both the reptation time of the micelles and the number of effective entanglements in the network. SANS measurements with contrast matching demonstrate that the nanoparticles do not disrupt the structure of the WLMs on length scales of the persistence length or less, which is also consistent with DLS measurements of the dynamics of the mixture. However, nanoparticle addition increases the osmotic compressibility of the WLM phase, which is consistent with the commensurate increase in mixture viscosity. DLS measurements also show that the nanoparticles diffuse through a medium with an effective viscosity greater than that of the mixture, which is again consistent with the nanoparticles being incorporated into the WLM network.

Focusing on the nanoparticle phase, the SANS measurements using surfactant contrast matching show the nanoparticles to be dispersed in the mixture and interacting with a potential of mean force that can be modeled by a square well potential. The strength of the interparticle attraction mediated by the WLMs is in semiquantitative agreement with the observed phase behavior and is consistent with the hypothesis of WLMs bridging nanoparticles. The dynamics and spatial arrangement of the nanoparticles in the WLM solutions are consistent with adsorption of the micelles onto the nanoparticles, which is likely to be due to hydrophobic interactions, as the surfactant and particles are of like charge.

A more quantitative agreement between the nanoparticle solution structure, dynamics, and phase behavior requires developing a more physical potential model for this unique system. The attractive potential of mean force acting between the nanoparticles that is thought to be mediated by bridging of wormlike micelles is novel and has not, to our knowledge, been solved theoretically. Consequently, we anticipate that our observations of the novel thermodynamics, rheology, and micromechanics of the nanoparticle surfactant mesophase will both provide a number of interesting observations for future investigations as well as motivate theoretical studies into the nature of WLM mediated interparticle interactions. Finally, we note that these results provide an initial road map for using nanoparticles as a means to control WLM solution rheology in industrial formulations.

Acknowledgment. We acknowledge Unilever Corporation for funding for this project. F.N. acknowledges partial support for his salary by the Alexander von Humboldt Foundation. We acknowledge the support of the National Institute of Standards and Technology, U.S. Department of Commerce, in providing the neutron research facilities used in this work. This work utilized facilities supported in part by the National Science Foundation under Agreement No. DMR-0454672.

(53) Kholodenko, A. L.; Douglas, J. F. *Phys. Rev. E* **1995**, *51*(2), 1081–1090.
(54) Abdel-Rahem, R. *Tenside, Surfactants, Deterg.* **2005**, *42*(2), 95–101.

Rheological measurements were performed on an instrument obtained under ARO award W911NF-05-1-0234. Any opinions, findings, and conclusions or recommendations expressed in this material are those of the author(s) and do not necessarily reflect the views of the Army Research Office.

Supporting Information Available: Autocorrelation functions of 100 mM CTAB/200 mM $NaNO_3$ in H_2O without and with 0.1 and 0.5 vol % silica particles and cryo-TEM micrographs of solutions containing 50 mM CTAB and 150 mM $NaNO_3$ and 50 mM CTAB, 150 mM $NaNO_3$, and 0.001 volume fraction silica particles. This material is available free of charge via the Internet at http://pubs.acs.org.

LA800271M